# Comparison of Recent Empirical Models of the Thermosphere

G.W. Prölss and P.W. Blum

Institut für Astrophysik
und Extraterrestrische Forschung
der Universität Bonn
D-5300 Bonn 1, F.R. Germany

ABSTRACT

To evaluate the accuracy of present-day thermospheric models, predictions of the C and MSIS-83 models were compared. To this end, the local time and seasonal variation of the predicted $N_2$ density were subjected to a Fourier analysis, and the amplitude and phase coefficients of the first four terms were represented as a function of latitude. A separate comparison of the model predictions was performed for each of these coefficients. Large differences of up to several 100% were observed at times, especially for the higher harmonics. However, these large discrepancies lead to only moderate uncertainties in the predicted $N_2$ density. Maximum deviations are of the order of 12% to 33%, depending on the components considered

Keywords: Upper Atmosphere, Thermospheric Models

## 1. INTRODUCTION

A sufficiently accurate knowledge of the air density in the upper atmosphere is essential for predicting the orbital decay of space debris. In the past, numerous thermospheric models have been published from which this information can be obtained. The most recent models are listed in Table 1. Not included are algorithms which address only certain aspects of the thermospheric density variations (e.g. Ref. 8-11).

All of these models are empirical in nature in that they are based on actual measurements rather than on theoretical calculations. Also, all of them use basically the same approach to model the thermospheric density. First, a height profile for the atmospheric temperature is adopted. Above 120 km altitude, for example, the DTM and MSIS-83 models use a Bates-type profile of the form (Ref. 12)

$$T(z) = T_\infty - (T_\infty - T(z_o))\, e^{-\sigma\zeta}$$

with $T$ = Temperature

$T_\infty$ = exospheric temperature

$z$ = height

$z_o$ = lower reference height = 120 km

$\sigma = (dT/d\zeta)_{z_o} / (T_\infty - T(z_o))$ = temperature gradient parameter

$\zeta = (z-z_o)(R_E+z_o)/(R_E+z)$ = geopotential height

$R_E$ = earth's radius

A very similar temperature profile is also used in the MSIS 77, ESRO 4 and C models (i.e. a Jacchia 64-type profile, see Ref. 13).

In a second step, a steady-state diffusion equation is assumed. Interactions between different constituents is neglected (e.g. Ref. 14):

$$\frac{1}{n_i}\frac{dn_i}{dz} + \frac{1}{H_i} + (1+\alpha_i)\frac{1}{T}\frac{dT}{dz} = 0$$

with $n_i$ = density of the $i^{th}$ atmospheric constituent

$H_i = kT/m_i g$ = scale height of the $i^{th}$ constituent, k being the Boltzmann constant, $m_i$ the mass of the $i^{th}$ constituent and g the acceleration of gravity

and $\alpha_i$ = thermal diffusion coefficient (equal to -0.4 for H and He and 0 otherwise).

Given the adopted temperature profile, this equation can be integrated to yield the height dependence of the various atmospheric constituents. For a Bates-type temperature profile, this integration can be performed analytically, yielding a Bates-Walker-type height profile for the density variation (Refs. 12,15):

$$n_i(z) = n_i(z_o)\,[T(z_o)/T(z)]^{1+\alpha_i+\gamma_i}\, e^{-\gamma_i\sigma\zeta}$$

with $\gamma_i = m_i g(z_o)/\sigma k T_\infty$

This kind of density height profile is adopted in all but the Jacchia 77 model.

In a third step, the dependence of the temperature and density on time, location, and geophysical conditions is modelled. To this end, the various parameters like the exospheric temperature and the lower boundary density are made variable with respect to these quantities. Thus in

Table 1

Recent Empirical Models of the Thermosphere

| Model | Year | Author(s) | Reference(s) |
|---|---|---|---|
| ESRO 4 | 1977 | von Zahn et al. | 1 |
| MSIS-77 | 1977 | Hedin et al. | 2,3 |
| J77 | 1977 | Jacchia | 4 |
| DTM | 1978 | Barlier et al. | 5 |
| C | 1980 | Köhnlein | 6 |
| MSIS-83 | 1983 | Hedin | 7 |

all models the exospheric temperature is made variable with respect to local time, season, latitude and solar and magnetic activity. Thereby spherical harmonics are used in all but the Jacchia model to describe the spatial-temporal variations. For a specific example, consider the following term which is used in the ESRO 4, MSIS 77, and MSIS-83 models to describe the diurnal (24 hour period) variation of the lower boundary density of the $i^{th}$ atmospheric constituent

$$n_i(z_o) = \overline{n_i(z_o)}\, e^{G_i}$$

with $\overline{n_i(z_o)}$ = average density at lower reference height $z_o$ and

$$G_i = F^i \{ [a^i_{11} P_{11} + a^i_{31} P_{31} + a^i_{51} P_{51} + (c^i_{11} P_{11} + c^i_{21} P_{21}) \cos \Omega (d - d^i_o)] \cos \omega\tau + [b^i_{11} P_{11} + b^i_{31} P_{31} + b^i_{51} P_{51} + (d^i_{11} P_{11} + d^i_{21} P_{21}) \cos \Omega (d - d^i_o)] \sin \omega\tau \}$$

where $F^i$ = function of solar activity

$a^i_{j1}$ = expansion coefficients

$P_{j1}$ = associated Legendre polynomials of order j,1 which depend only on latitude

$\Omega$ = $2\pi/365d$ = annual frequency

$d; d^i_o$ = day of the year; phase (delay time) coefficient

$\omega$ = $2\pi/24h$ = diurnal frequency

$\tau$ = local time, hours

A similar ansatz is also made in the DTM and in the C model. In the DTM model, however, the solar activity dependence of the diurnal component is neglected ($F^1$=1) and in the C model an additional height dependence factor is introduced to account for deviations from diffusive equilibrium.

As can be seen from this example, the actual model formulation is quite complex and requires a large number of coefficients. In fact, the MSIS-83 model uses more than 750 coefficients to describe the behavior of the temperature and of five atmospheric constituents.

This is of no immediate concern to the potential user as long as the required software is obtained directly from the respective author. Of immediate interest, however, is the question as to which of the numerous models should be used and what accuracy can be expected. In regard to the first question, we note that the most recent models are based on the largest amount of data and use the most sophisticated algorithms. Therefore in most cases the C model and the MSIS-83 model should be preferred.

As for the second question concerning the accuracy of these models, a proper evaluation is much more difficult. One way to find out would be to compare model predictions with actual measurements (e.g. Refs. 16,17). No final results are expected from this procedure, however, since the measured data sets themselves are usually not free from errors. Another possible way is to compare model predictions among themselves (e.g. Refs. 18,19,20,21). This latter approach was also taken in the present study. Here it is assumed that differences in the model predictions are a fair measure of the uncertainties to be expected.

## 2. METHOD OF ANALYSIS

A comprehensive comparison of different models is a fairly large undertaking. It would include predictions made for the temperature and for the different gas constituents. Also, it would consider predictions for different heights, different local times, different seasons, different latitudes (and partly longitudes) and for different levels of solar and geomagnetic activity. Such a comprehensive evaluation is far beyond the scope of the present contribution. Rather, a fairly restricted comparison is presented, as is indicated in Table 2. First, only the C model and the MSIS-83 model are considered, which represent the

Table 2

Model Comparison

| | |
|---|---|
| Models | C and MSIS-83 |
| Constituents | $N_2$ |
| Altitudes | 300 and 150 km |
| Longitude/UT effects | neglected |
| Geophysical conditions | $F10.7 = \overline{F10.7} = 100$; $Kp = 1_o / Ap = 4$ |
| Variations considered | 1. local time variations as a function of latitude on April 1<br>2. seasonal variations as a function of latitude at 3 LT |

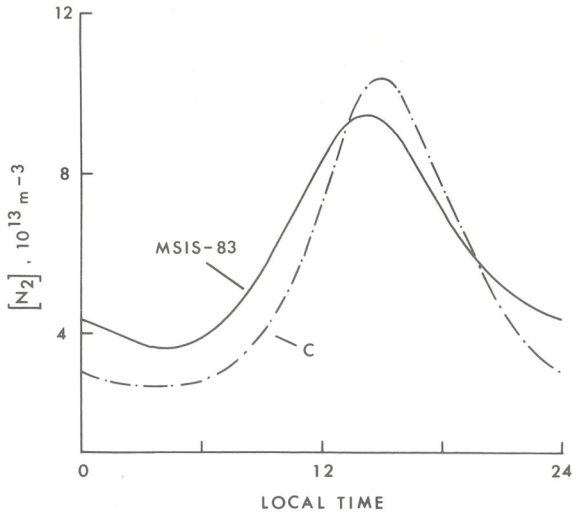


Figure 1 Average local time variation of the $N_2$ density at 300 km altitude and 30°S latitude on April 1 as specified by the C and MSIS-83 models.

most advanced algorithms. Second, only predictions for the molecular nitrogen density are compared. It is the major constituent in the lower thermosphere and also a good indicator of the upper atmospheric temperature. Third, only two heights are considered: 300 km corresponds to the height with the largest data coverage and 150 km corresponds to the lower boundary of satellite measurements. Fourth, only zonal averages are considered in the sense that any longitudinal and/or UT effects are neglected. Finally, only constant geophysical conditions are considered. Explicitly moderate solar and low magnetic activity is assumed. What remains then are changes with latitude, local time and season. In the following, the latitude dependence of the local time variation at equinox and the seasonal variation at 3 local time will be compared. Figure 1 illustrates the possible form of such a comparison. Here the local time variation of the $N_2$ density as predicted by the C and MSIS-83 models is presented. It is evident that the general run of these curves is quite similar, even though differences of up to 30% are observed near midnight.

This kind of comparison can provide a rough idea as to the general accuracy to be expected from these models. However, a better understanding of these differences is obtained through a more detailed study using a Fourier analysis of the temporal variations (e.g. Refs. 16,21). Thus the local time variation, as shown for example in Fig. 1, was decomposed into a daily mean value and a diurnal, semidiurnal and terdiurnal component. Subsequently, the daily mean values as predicted by the two models were compared separately and so were the first three harmonics. Similarly, the seasonal variation was decomposed into an annual mean value and an annual, semiannual and terannual component; again, these terms were compared separately. In each case, the time variation of the $N_2$ density is represented by a Fourier series of the form

$$n(\phi,t) = a_o(\phi) + a_1(\phi)\cos[\omega(t-t_1(\phi))] + a_2(\phi)\cos[2\omega(t-t_2(\phi))] + a_3(\phi)\cos[3\omega(t-t_3(\phi))] + \ldots$$

with $n$ = $N_2$ number density

$\phi$ = latitude

$t$ = time (in hours for local time variations, in days for seasonal variations

$\omega$ = fundamental frequency = $\begin{cases} 2\pi/24h \text{ for local time variations} \\ 2\pi/365d \text{ for seasonal variations} \end{cases}$

and $a_i, t_i$ = amplitude and phase coefficients

It is on the basis of the expansion coefficients $a_i$ and $t_i$ and their latitude dependence that the predictions of the C and MSIS-83 models are compared in the following. Incidently, these coefficients cannot be obtained directly from the model algorithms because there they enter through different terms (e.g. $T_\infty$, $n(z_o)$) and also in a non-linear fashion (see expansion for $n(z_o)$ given above).

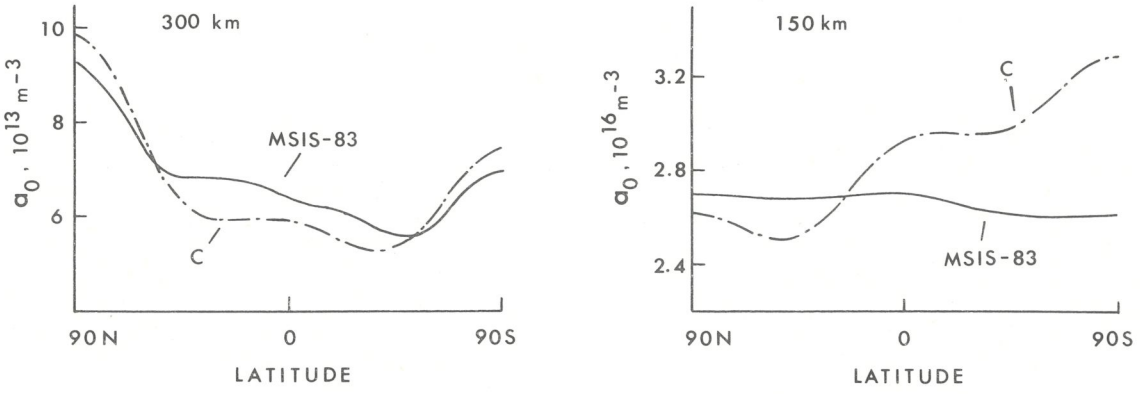


Figure 2 Latitude dependence of the $N_2$ daily mean value at 300 and 150 km altitude on April 1 as specified by the C and MSIS-83 models.

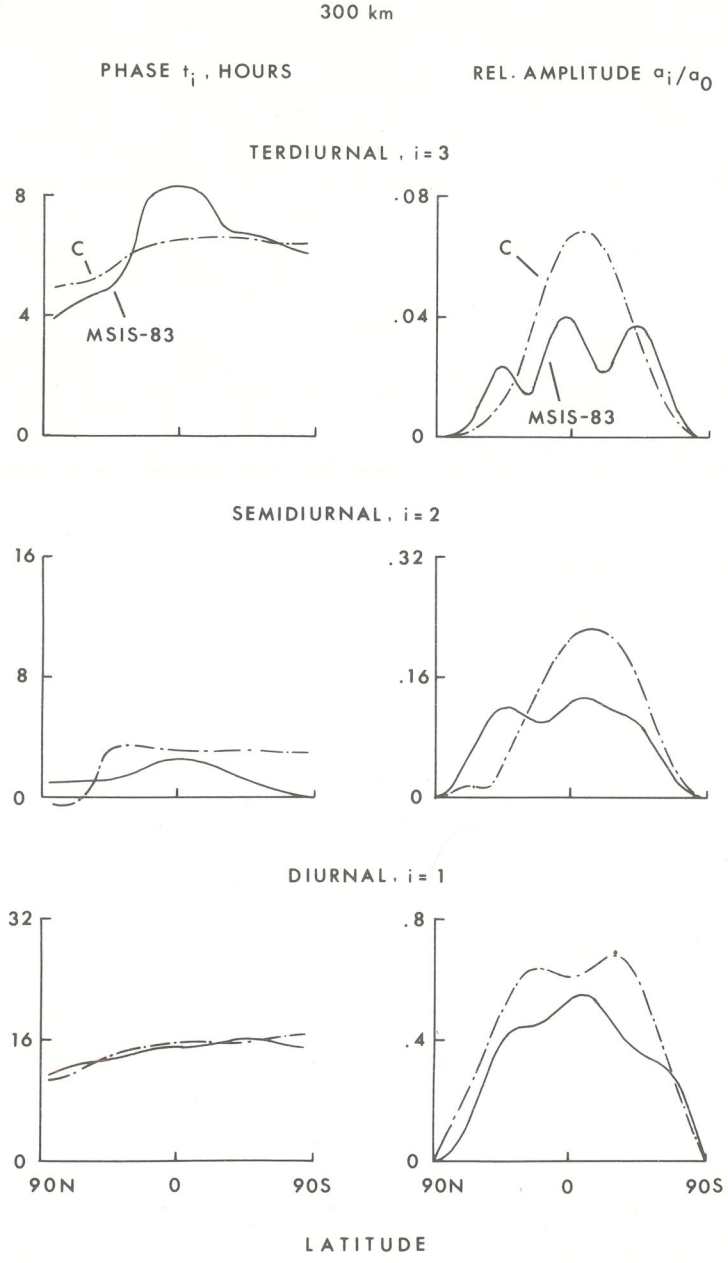


Figure 3 Latitude dependence of the diurnal, semidiurnal, and terdiurnal $N_2$ density variation at 300 km altitude on April 1 as specified by the C and MSIS-83 models.

## 3. RESULTS

### 3.1 Local time variations

Figure 2 shows the latitudinal variation of the time independent term $a_0$ which for the local time variation corresponds to the daily mean value. As is evident, at 300 km altitude there is good agreement between the magnitude and latitudinal structure predicted by both models, and deviations are less than 13%. Both models predict daily mean values which are higher at the poles than at the equator and also higher at the North Pole than at the South Pole. This latter asymmetry is due to the fact that on April 1 the subsolar point has already migrated into the northern hemisphere.

Poorer agreement is observed in the lower thermosphere. At 150 km altitude, significant differences in the latitudinal variation and in the predicted magnitude of the mean value (up to 25% at the South Pole) are evident. It is tempting to attribute this deterioration to the poorer data coverage in this region. Later examples, however, show that this trend is not uniform.

As for the time dependent terms, Figs. 3 and 4 show the relative amplitudes and phases of the diurnal, semidiurnal and terdiurnal components

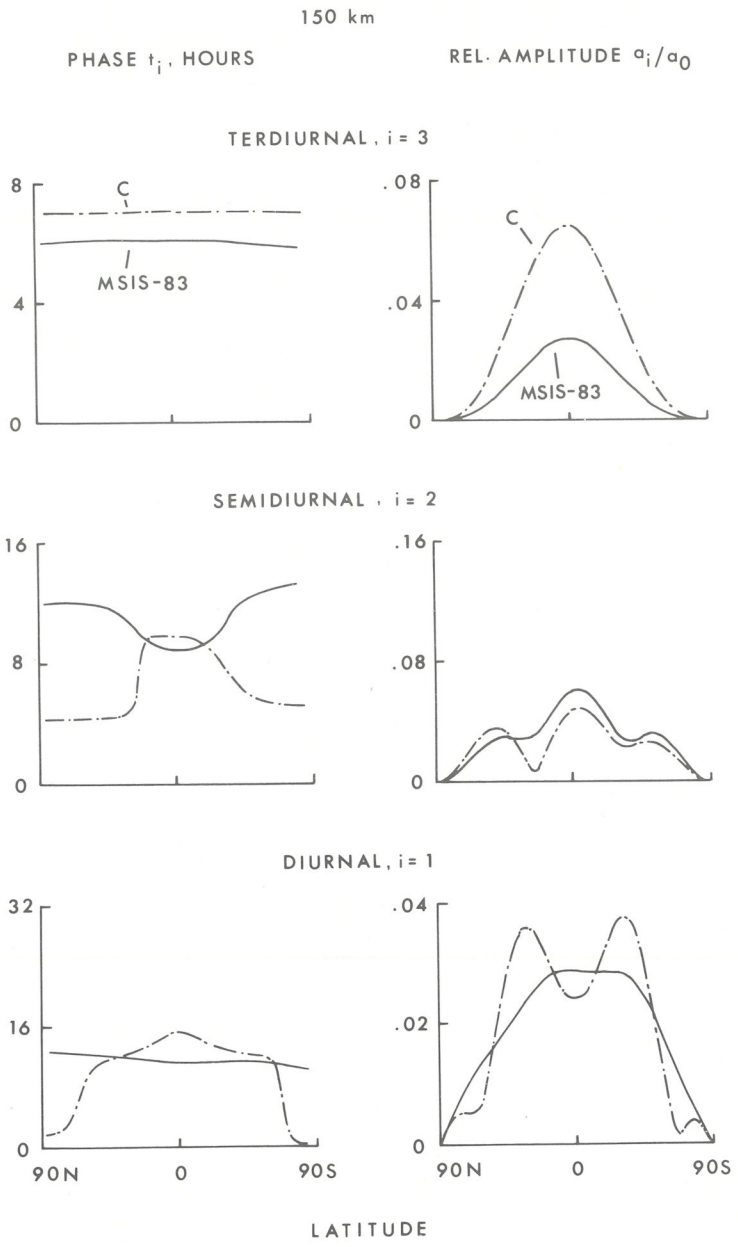


Figure 4 Same as Fig. 3 for an altitude of 150 km.

as a function of latitude. With an amplitude of up to 60%, the diurnal component clearly dominates the local time variation at 300 km altitude. It is to be compared with the 10 to 20% and 4 to 7% maximum amplitude of the semidiurnal and terdiurnal component. The basic latitudinal variation follows from the fact that the local time dependence disappears at the poles and reaches a maximum somewhere at lower latitudes.

Comparing the two model predictions, significant differences are evident. This concerns both the latitudinal structure and the magnitude of the amplitudes. In reference to the MSIS-83 model, maximum differences are of the order of 70% for the diurnal and semidiurnal variations and up to 200% for the terdiurnal variation. For the large diurnal component, this translates into uncertainties in the $N_2$ density prediction of up to 27% and somewhat less for the semidiurnal (≤9%) and terdiurnal (≤4%) variations.

In contrast, acceptable agreement is observed for the phases of the semi- and terdiurnal components, and even excellent agreement for the diurnal variation. In this latter case, both models predict a maximum in the $N_2$ density at 16 hours in the southern hemisphere and somewhat earlier in the northern hemisphere.

Descending in height, the significance of the local time variation rapidly decreases. This is illustrated in Fig. 4, which indicates that at 150 km altitude the maximum amplitude of the diurnal variation has dropped to below the 4% level. Indeed, it has become smaller than the semi-

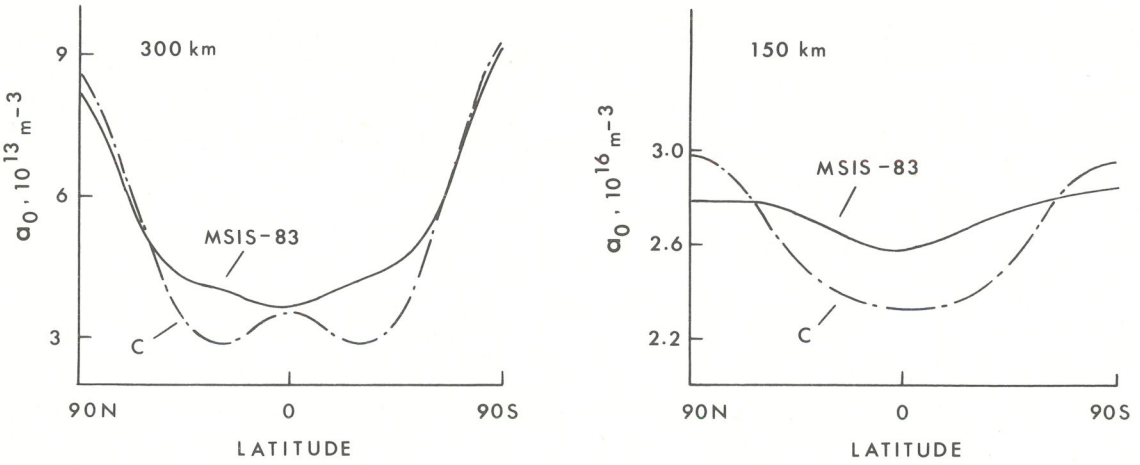


Figure 5 Latitude dependence of the $N_2$ annual mean value at 300 and 150 km altitude at 3 o'clock in the morning as specified by the C and MSIS-83 models.

diurnal component which, however, is but a few percent larger.

Again comparing the model predictions, we find good agreement for the latitudinal structure of the semi- and terdiurnal variations but significant differences for the diurnal component. Indeed, it appears doubtful that the oscillatory changes predicted by the C model have a physical basis. In regard to the magnitude of the amplitudes, larger deviations are observed for all three components, with maximum differences of the order of 57%, 80%, and 140% for the diurnal, semidiurnal and terdiurnal variations, respectively. Because local time variations are small at these heights, the relatively large discrepancies do not result in significant errors in the predicted density ($\leq$4%). For the same reason, any differences in the phase predictions will not have any significant effect on the model accuracy.

3.2 Seasonal variations

As was the case for the local time variations, seasonal changes were decomposed into a time independent term and the first three harmonics. Figure 5 shows the latitudinal variation of the time independent term $a_o$ which this time corresponds to the annual mean value. As is evident, at 300 km altitude and in the early morning sector large latitudinal variations of more than 100% are observed. Maximum values are found at the poles; this has to do with the local time sector considered which influences the low latitude values. Comparing the two model predictions, excellent agreement is observed at high and low latitudes, but larger differences (up to 33%) at middle latitudes. Contrary to expectations, the overall agreement does not deteriorate in the lower thermosphere, and maximum deviations are less than 12% at 150 km altitude.

Figures 6 and 7 show the latitudinal variation of the time dependent terms. At 300 km altitude, the most striking feature is the large annual variation, reaching a maximum amplitude of 80% at the South Pole. There is also a distinct asymmetry between the North and South Pole amplitudes which is attributed to an increased energy deposition in the southern polar region (e.g. Ref. 22). In comparison, the semiannual variation is fairly small, reaching a maximum amplitude of 15%. It is this component, however, which is very important for satellite ephemeris predictions. As for the terannual variation, only the C model indicates a significant amplitude of 8% at the South Pole. Incidently, none of the models presently available includes specific terms for the terannual variation, but these changes are introduced through the nonlinearities of the model algorithms.

Comparing the latitudinal structure of the amplitudes, excellent agreement is found for the annual and also partly for the semiannual component. In contrast, predictions for the terannual variation are quite different. As for the magnitudes of the amplitudes, significant deviations are observed for all three components, reaching maximum values of 35%, 130%, and even 350% for the annual, semiannual and terannual variations, respectively. This results in maximum uncertainties of 15% in the density predictions for the annual component and 6% for both the semiannual and terannual components. As before, all percentage values refer to the MSIS-83 model.

Comparing the predicted phases, fairly good agreement is found for the latitudinal structure of all three components. This is also true for the annual component in the southern hemisphere, where model predictions differ by close to 365 days. With respect to the magnitude of the predicted time delays, larger differences are observed for the semiannual component ($\sim$40 days at the South Pole) and for the terannual variation ($\sim$25 days in the southern hemisphere).

As was the case for the local time variation, a significant decrease of the seasonal changes is observed in the lower thermosphere (Fig. 7). Model predictions, however, are far from uniform in this region. This is true for both the magnitude and the latitudinal variations of the coefficients. For example, maximum deviations as large as 110%, 170% and even 800% are observed for the amplitudes of the annual, semiannual and terannual components. This causes uncertainties of up to 14% in the density predictions for the annual and semiannual components and less for the

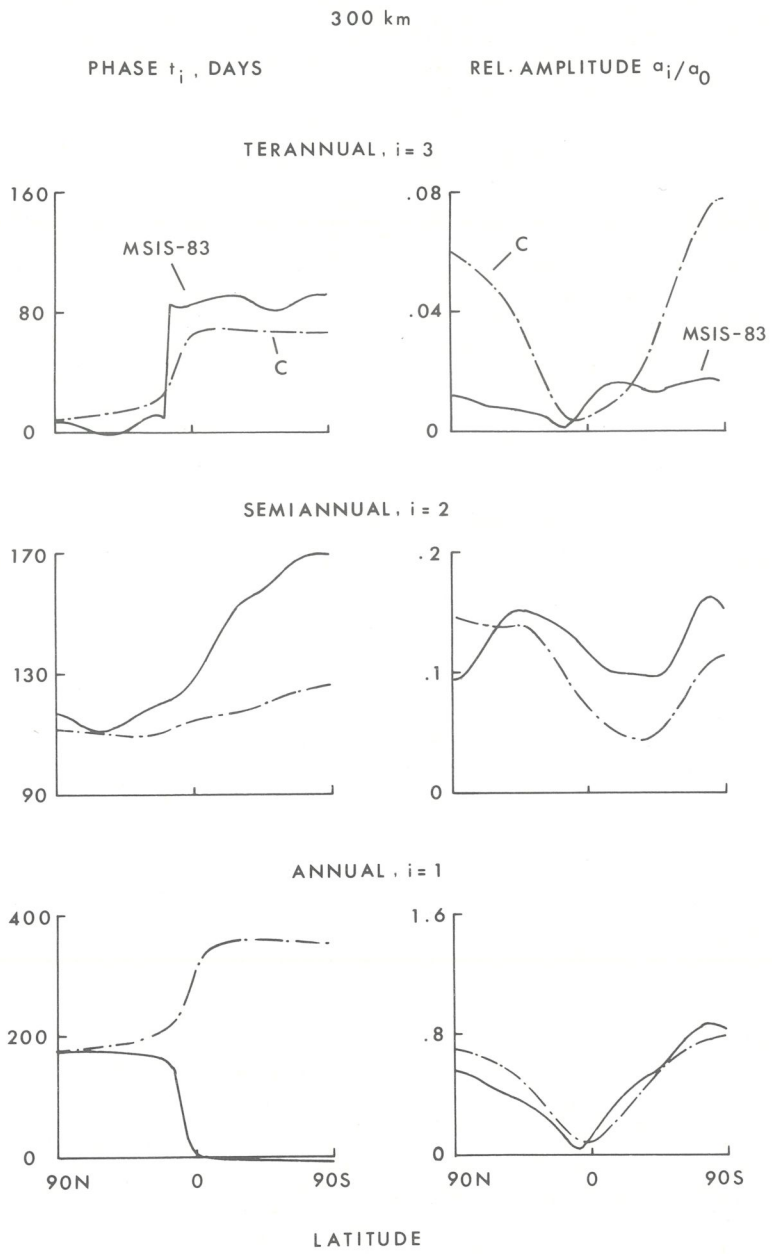


Figure 6 Latitude dependence of the annual, semiannual, and terannual $N_2$ density variation at 300 km altitude and at 3 o'clock in the morning as specified by the C and MSIS-83 models.

terannual variation. Also, some of the oscillations predicted for the latitudinal structure appear to be artificially introduced by the model algorithms. With respect to the phases, differences of up to 70, 30 and 40 days are found for the first three harmonics, respectively. Evidently, in going from the higher to the lower thermosphere the accuracy of the model predictions has deteriorated.

## 4. CONCLUSIONS

The following conclusions can be drawn from the model comparison presented in Figs. 2 to 7. First, these graphs clearly indicate the significance and morphology of various upper atmospheric variations. This way a better understanding of the physics of the upper atmosphere is obtained. Second, they point to certain deficiencies of the model algorithms considered. This way the modelling of the upper atmosphere can be improved. And third, they indicate the accuracy of the model predictions. This way a more realistic model evaluation is achieved.

With respect to the accuracy, it is shown that significant differences may exist between the model predictions. Not surprisingly, these deviations are largest for the smallest variations considered. Fortunately, here they do not cause

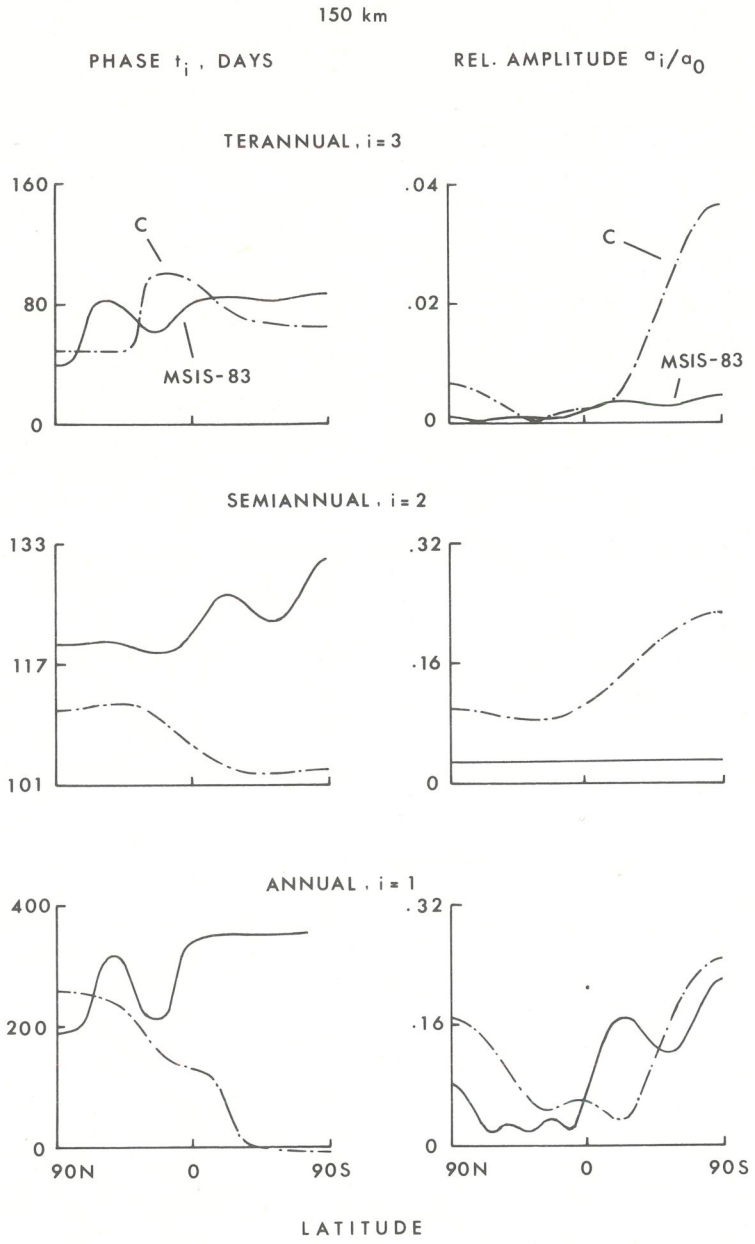


Figure 7 Same as Fig. 6 for an altitude of 150 km.

larger uncertainties in the predicted $N_2$ density. For example, the predicted amplitudes of the terannual variation at 150 km differ by up to 800%. Because this component is small, differences in the predicted $N_2$ density are less than 4%. More critical are the time independent (mean) values because here deviations cause equally large differences in the predicted $N_2$ density. Maximum deviations observed for this component range between 12% and 33% (Figs. 2 and 5). Uncertainties of similar magnitude are also associated with the dominant time dependent terms. Here maximum differences in the predicted $N_2$ density are 27% for the diurnal component at 300 km altitude (Fig. 3), 16% for the annual component at 300 km altitude (Fig. 6), and 14% for the annual and semiannual variation at 150 km height (Fig. 7). These values may be considered a good measure for the overall accuracy of present-day models. In this respect, they are in good agreement with estimates based on a direct comparison between model predictions and actual measurements (e.g. Refs. 6,17). In these studies average deviations of the order of ±20% are quoted.

It is important to realize that the above error estimates apply only to regular variations in the undisturbed thermosphere. However, there do exist very significant irregular variations which are caused by the stochastic dissipation of solar wind energy in the polar atmosphere. These effects are very difficult to model, and introduce an additional element of uncertainty (e.g. Refs. 23,24,25,26). Thus during a magnetospheric storm, model predictions may be off by far more than 20%. The influence such an event may have on the re-entry of space debris is discussed in Ref. 27.

Acknowledgments: The contributions to this study by K.G.H. Schuchardt and W. Kurtsiefer are gratefully acknowledged.

REFERENCES

1. von Zahn U et al 1977, ESRO 4 model of global thermospheric composition and temperatures during times of low solar activity, Geophys Res Lett 4, 33-36.

2. Hedin A E et al 1977, A global thermospheric model based on mass spectrometer and incoherent scatter data MSIS 1, $N_2$ density and temperature, J Geophys Res 82, 2139-2147.

3. Hedin A E et al 1977, A global thermospheric model based on mass spectrometer and incoherent scatter data MSIS 2, Composition, J Geophys Res 82, 2148-2156.

4. Jacchia L G 1977, Thermospheric temperature, density, and composition: new models, Smithson Astrophys Obs Spec Rept 375, Cambridge, Mass.

5. Barlier F et al 1978, A thermospheric model based on satellite drag data, Ann Géophys 34, 9-24.

6. Köhnlein W 1980, A model of thermospheric temperature and composition, Planet Space Sci 28, 225-243.

7. Hedin A E 1983, A revised thermospheric model based on mass spectrometer and incoherent scatter data: MSIS-83, J Geophys Res 88, 10170-10188.

8. Blum P W et al 1978, Semi-empirical models of the neutral atmosphere based on turbopause height and exospheric temperature variations, J Atmos Terr Phys 40, 1131-1135.

9. Köhnlein W et al 1979, A thermospheric model of the annual variations of He, N, O, $N_2$ and Ar from the AEROS Nims data, J Geophys Res 84, 4355-4362.

10. Engebretson M J et al 1980, Diurnal, seasonal, and nighttime variations of atomic nitrogen in the equatorial thermosphere, J Geophys Res 85, 2165-2170.

11. Stehle C G et al 1982, A global model of the neutral thermosphere in magnetic coordinates based on OGO 6 data, J Geophys Res 87, 1615-1622.

12. Bates D R 1959, Some problems concerning the terrestrial atmosphere above about the 100-km level, Proc Roy Soc London A253, 451-462.

13. Jacchia L G 1964, Static diffusion models of the upper atmosphere with empirical temperature profiles, Smithson Astrophys Obs Spec Rept 170, Cambridge, Mass.

14. Banks P M & Kockarts G 1973, Aeronomy B, New York and London, Academic Press, 33-36.

15. Walker J C G 1965, Analytic representation of upper atmosphere densities based on Jacchia's static diffusion models, J Atmos Sci 22, 462-463.

16. Kasprzak W T & Newton G P 1976, Comparison of measured and theoretical thermospheric daily composition variations, J Geophys Res 81, 2405-2409.

17. Prölss G W & Roemer M 1986, Comparison of the ESRO 4 thermosphere model with ESRO 4 data during geomagnetically quiet conditions, Proc ESA Workshop on Re-entry of Space Debris, ESOC Darmstadt, F.R. Germany, 24-25 Sept. 1985, this issue.

18. von Zahn & Fricke K H 1978, Empirical models of global thermospheric composition and temperature during geomagnetically quiet times compared with ESRO 4 gas analyzer data, Rev Geophys Space Phys 16, 169-175.

19. Barlier F et al 1979, Comparisons between various semi-empirical thermospheric models of the terrestrial atmosphere, J Atmos Terr Phys 41, 527-541.

20. Barlier F & Berger C 1983, A point of view on semi-empirical thermospheric models, Planet Space Sci 31, 945-966.

21. Schuchardt K G H et al 1985, A comparison of semi-empirical models in the lower thermosphere, Adv Space Res 5(7), 183-192.

22. Barlier F et al 1974, North-South asymmetries in the thermosphere during the last maximum of the solar cycle, J Geophys Res 79, 5273-5285.

23. Prölss G W 1980, Magnetic storm associated perturbations of the upper atmosphere: recent results obtained by satellite-borne gas analyzers, Rev Geophys Space Phys 18, 183-202.

24. Thuillier G et al 1980, Magnetic activity effects on the exospheric temperatures at high latitudes, J Atmos Terr Phys 42, 653-660.

25. Hedin A E et al 1981, Semiempirical modeling of thermospheric magnetic storms, J Geophys Res 86, 3515-3518.

26. Prölss G W & Roemer M 1985, Some properties of the polar energy source and of the associated atmospheric perturbations, Adv Space Res 5(7), 193-202.

27. Schuchardt K G H et al 1986, Anomalous perigee shift and eccentricity variation due to air drag in the re-entry phase, Proc ESA Workshop on Re-entry of Space Debris, ESOC Darmstadt, F.R. Germany, 24-25 Sept. 1985, this issue.